The Journal of Experimental Biology 202, 2893–2909 (1999)
Printed in Great Britain © The Company of Biologists Limited 1999
JEB2242

DIRECTIONAL ACOUSTIC RADIATION IN THE STRUT DISPLAY OF MALE SAGE GROUSE *CENTROCERCUS UROPHASIANUS*

MARC S. DANTZKER[1,*], GRANT B. DEANE[2] AND JACK W. BRADBURY[1]

[1]*University of California, San Diego, Department of Biology, 9500 Gilman Drive, La Jolla, CA 92093-0116, USA* and [2]*Marine Physical Laboratory, Scripps Institute of Oceanography, La Jolla, CA 92093-0238, USA*

*e-mail: mdantzker@ucsd.edu

Accepted 11 August; published on WWW 13 October 1999

Summary

We present evidence that the acoustic component of the strut display of male sage grouse *Centrocercus urophasianus* is highly directional and that the nature of this directionality is unique among measured vertebrates. Where vertebrate acoustic signals have been found to be directional, they are most intense anteriorly and are bilaterally symmetrical. Our results show that sage grouse acoustic radiation (beam) patterns are often asymmetric about the birds' anterior–posterior axis. The beam pattern of the 'whistle' note is actually strikingly bilobate with a deep null directly in front of the displaying bird. While the sage grouse display serves to attract potential mates, male sage grouse rarely face females head on when they call. The results of this study suggest that males may reach females with a high-intensity signal despite their preference for an oblique display posture relative to those females. We characterized these patterns using a novel technique that allowed us to map acoustic radiation patterns of unrestrained animals calling in the wild. Using an eight-microphone array, our technique integrates acoustic localization with synchronous pressure-field measurements while controlling for small-scale environmental variation in sound propagation.

Key words: sage grouse, *Centrocercus urophasianus*, strut display, acoustic communication, mate attraction, directionality, beam pattern, lek, airsac, acoustic radiation pattern, environmental acoustics, sound propagation, sound production, directivity index.

Introduction

Studies of acoustic mate-attraction displays have concentrated on the role of spectral and temporal characteristics in signal evolution. Despite the likely importance of signal directionality (Bradbury and Vehrencamp, 1998; Witkin, 1977), the fitness consequences of directional patterns of acoustic display have been largely overlooked because these patterns have been considered too difficult to map in the field. In this paper, we present measures of the acoustic radiation (beam) patterns of the male sage grouse strut display. The spectral and temporal aspects of this display have been extensively examined (Gibson, 1996; Gibson and Bradbury, 1985; Gibson et al., 1991; Hartzler, 1972; Spurrier et al., 1994; Wiley, 1973a; Young, 1994). However, despite anecdotal observations of strong directionality (Wiley, 1973a; J. W. Bradbury and M. S. Dantzker, personal observation), these directional patterns have not been quantified and their consequences have not been explored.

The strut display of the male sage grouse is highly stereotyped and elaborate (Hjorth, 1970; Honess and Allred, 1942; Wiley, 1973a; Young et al., 1994). Prior to display, a male sage grouse inflates a region of his esophagus that sits in a muscular bag at the base of his neck. The strut display is a series of three heaves of this esophageal expansion through outreached wings held stiffly at either side (Fig. 1). Sage grouse keep their beak closed for most of the display; sound production coincides instead with tandem anterior expansions of the esophageal air sac through ventral apteria (featherless regions) on the neck (Hjorth, 1970; Young et al., 1994). These dark, inflated skin patches bulge repeatedly through a dense region of white feathers to create a dramatic and unusual acoustic (Fig. 2) and visual (Fig. 1) display. While many other groups of vertebrates use external air sacs in sound production and radiation, this explosive use of dual anterior air sacs is unique to the *Centrocercus* grouse strut display. This mate-attraction display has evolved under the intense sexual selection of a lek mating system (Höglund and Alatalo, 1995). However, male sage grouse do not appear to direct their display efforts towards females by facing them during display (Simon, 1940; Wiley, 1973a). In this study, we examine the directionality of the acoustic signal produced by this unusual display mechanism of sage grouse.

Directional patterns of acoustic radiation, beam patterns, have usually been measured under laboratory conditions where the animal's position and orientation are held constant and repeated measurements are made on induced or coaxed phonation. Similar methods can be used in the field when the animals of interest remain stationary during display and will tolerate movements around them (Gerhardt, 1998). Sage

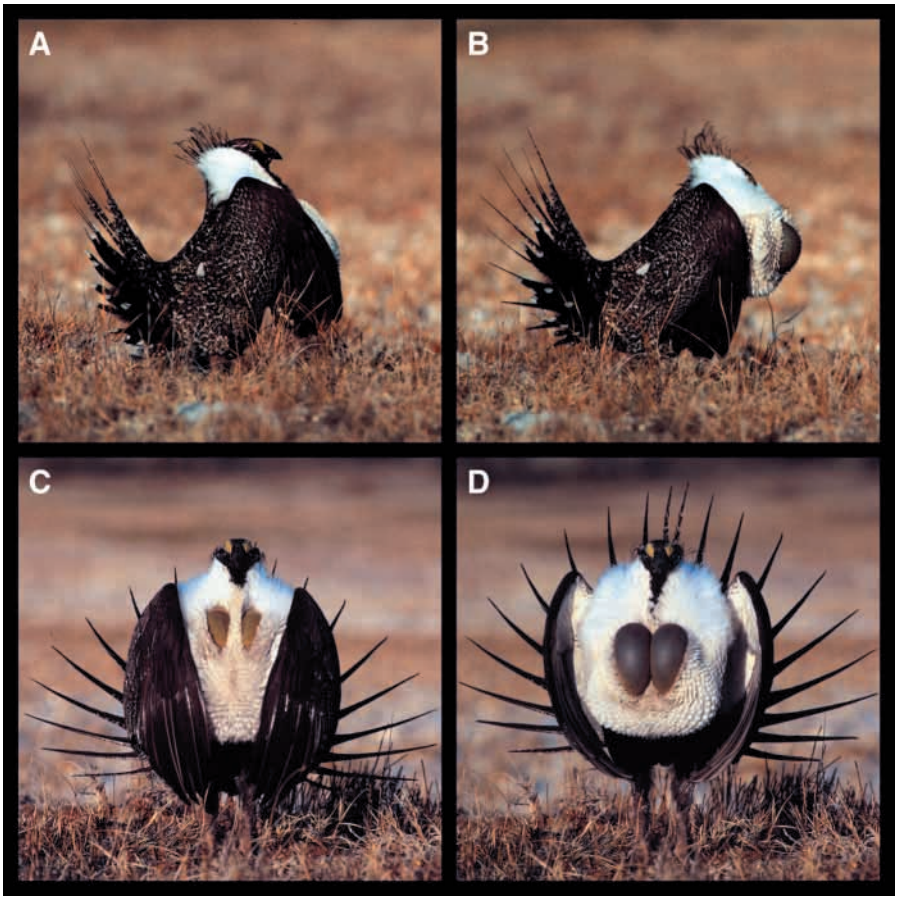

Fig. 1. Strut display of male sage grouse. (A) Profile with white esophageal sac held behind the two outstretched wings. (B) Profile with sac fully expanded and visible through the anterior apterium on the sac. Note that the head is no longer visible. (C) Pre-expansion thrust of the air sac from the front. The apteria are visible but not distended. (D) Full expansion of the apteria, accompanied by an opening of the wings. Note that the expanded apteria touch along the midline. The exposed air sacs and the beak face forwards for the duration of the strut. The vegetation at the male's feet is typical of the lek. All exposures are either 1/4000 s or 1/8000 s.

grouse afford neither such opportunity as they are rarely available for captive study and wild birds travel rapidly around their territories between consecutive displays. We developed a novel method for the measurement and calculation of these beam patterns which allows for the use of unrestrained and actively mobile wild individuals while correcting for heterogeneity in the acoustic environment.

Here, we present evidence that acoustic radiation patterns of the sage grouse strut display are unlike any previously measured in a vertebrate. Where vertebrate acoustic signals have been found to be directional, they are most intense anteriorly and are bilaterally symmetrical (see Discussion). Our results show that sage grouse beam patterns are variably asymmetric about the animal's anterior–posterior axis. The beam pattern of one of the call elements, the 'whistle', has a deep minimum (null) directly in front of the displaying bird and is instead most intense to the sides and behind.

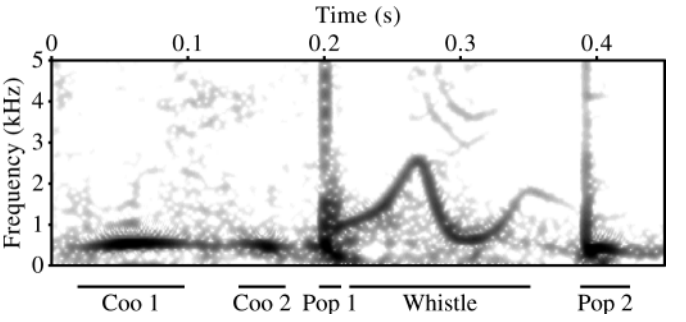

Fig. 2. Spectrogram of the acoustic component of a male sage grouse strut display showing the time limits of each note as well as the notes' names as used by Gibson and Bradbury (1985) and Wiley (1973a). Spectrogram parameters: frame size, 512 point; sampling rate, 22.5 kHz; windowing function, Hanning; frame overlap, 94 %.

Materials and methods

Sage grouse *Centrocercus urophasianus* (Bonaparte) travel across the mostly flat display arena (lek) on foot; therefore, we focused our efforts on characterizing acoustic directionality in the horizontal plane. The sound field surrounding an acoustic source, in this case a strutting sage grouse, is considered to be directional when the amplitudes of the induced pressure waves vary as a function of angle. This angular variation is described by a normalized function called the beam pattern (Kinsler et al., 1982, p.175). Here, we describe a method for measuring beam patterns of unrestrained animals in complicated acoustic environments.

Measurement summary

We recorded male sage grouse using an eight-microphone array that we deployed around their display territories

(described in greater detail below). The essential problem we faced in determining the beam pattern from these recordings was to separate the superimposed effects of source directionality, which were inherent to the calling bird, and directionality introduced by the environment. In our case, this environmental effect arose primarily from interfering acoustic reflections from the lek surface. To discriminate between the directional effects of the source and those that were environmentally induced, we measured the directionality of the signal received from a known, calibrated source positioned inside our array. This calibration procedure allowed us to identify and quantify the effects of the environment across the range of frequencies used by the sage grouse. We could then calculate beam patterns generated only by the directional properties of the source. The mathematical basis underlying our calibration procedure, as well as the concept of beam pattern relevant to this study, are developed in some detail below.

Beam pattern and the directional factor

In the far field, the pressure field in a horizontal plane, $p_s(r,\theta)$, can be expressed as a function of distance, r, and horizontal angle, θ, from the sound source such that:

$$p_s(r,\theta) = p_{s,axis}(r)H(\theta)\,. \quad (1)$$

$H(\theta)$ is the directional factor that has been normalized so that the maximum value is unity (Kinsler et al., 1982). The value of θ for which $H(\theta)=1$ defines the acoustic axis of the radiation pattern. The term $p_{s,axis}(r)$ is the far-field pressure on the acoustic axis. Therefore, $p_{s,axis}(r)$ is dependent on both range and source level, while $H(\theta)$ is dependent only on angle. The directional factor is usually represented as its decibel (dB) equivalent, the beam pattern, $b(\theta)$ (Kinsler et al., 1982) using:

$$b(\theta) = 10\log H^2(\theta)\,, \quad (2)$$

where the maximum value of the beam pattern, $MAX[b(\theta)]$, is 0 dB.

In general, both source strength and directionality vary with frequency of vibration, f. Accordingly, the directional factor, $H(f,\theta)$, is most generally expressed as function of both angle and frequency, a convention we will adopt. Additionally, since the directional factor is independent of distance, equation 1 can be rewritten for a fixed distance such that:

$$p_s(f,1,\theta) = p_{s,axis}(f,1)H(f,\theta)\,, \quad (3)$$

where r is 1 m and is the directional factor now normalized so that each frequency component has a corresponding value of θ, where $H(f,\theta_{max})=1$. We further define θ as the horizontal clockwise angle with respect to the bird's anterior–posterior axis, where $\theta=1$ directly in front of the displaying bird. Here, $p_s(f,1,\theta)$ is the free-field pressure field 1 m from the sound source (bird) measured as a function of frequency and angle. The pressure 1 m from the source on the acoustic axis is $p_{s,axis}(f,1)$, which reflects the frequency-dependence of the source level. It follows that for any one frequency:

$$p_{s,axis}(f,1) = MAX[p_s(f,1,\theta)]\,. \quad (4)$$

In a controlled setting, where interfering acoustic returns from the environment can be eliminated, the free-field values of $p_s(f,1,\theta)$ can be measured directly. From this, one can calculate the directional factor and a beam pattern for each frequency component. In contrast, our experimental design measures the acoustic field around a grouse calling just above the ground. Sound propagation near the ground is complicated by interference from multiple acoustic reflections. It is therefore necessary to correct for the transmission loss in order to determine the free-field values of $p_s(f,1,\theta)$.

The free-field source sound pressure field 1 m from the bird, $p_s(f,1,\theta)$, can be determined from measures of the acoustic field using:

$$p_s(f,1,\theta) = \frac{p_r(f,r,\theta)}{TL(f,r,\theta)}\,, \quad (5)$$

where $p_r(f,r,\theta)$ is the measured sound pressure, including all transmission effects, and $TL(f,r,\theta)$ is the transmission loss across the same propagation path. Previous field studies of source directionality have used a homogeneous geometric spreading model for transmission loss which is independent of frequency, $TL(r)=1/r$, and identical across all paths of equal distance (Archibald, 1974; Bennet-Clark, 1987; Forrest, 1991; Gerhardt, 1975; Narins and Hurley, 1982; Witkin, 1977). Our preliminary examination of sound propagation over the lek revealed that models such as this were insufficient for this environment. Therefore, we empirically measured the transmission loss curves for each propagation path (see Appendices A and B).

It is now possible, from equations 3, 4 and 5, to derive an equation for the directional factor $H(f,\theta)$ from the measures of the pressure field gathered by our receiver array and the independently measured transmission loss curves for each propagation path. This is:

$$H(f,\theta) = \frac{\dfrac{p_r(f,r,\theta)}{TL(f,r,\theta)}}{MAX\left[\dfrac{p_r(f,r,\theta)}{TL(f,r,\theta)}\right]}\,. \quad (6)$$

The two-dimensional directional factor $H(f,\theta)$ is cumbersome to visualize. It is helpful to extract the frequency-dependence by calculating a narrow-band average. As long as the band of frequencies is narrow, this simplification is appropriate. To do this, we calculate a band-averaged power Π_{band} using:

$$\Pi_{band}(\theta) = \frac{1}{\Delta f}\sum_{f_0}^{f_1}\frac{|p_r(f,r,\theta)|^2}{TL^2(f,r,\theta)}\,, \quad (7)$$

where $|p_r(f,r,\theta)|^2$ is the squared modulus of the pressure measurements, the power spectral density. This allows us to calculate a measure of the band-averaged squared directional factor, $H_{band}^2(\theta)$, using:

$$H_{band}^2(\theta) = \frac{\Pi_{band}(\theta)}{MAX[\Pi_{band}(\theta)]}\,. \quad (8)$$

From this, we can define the band-averaged beam pattern as:

$$b_{\text{band}}(\theta) = 10\log H_{\text{band}}^2(\theta)\,. \quad (9)$$

The samples of the acoustic field, $p_r(f,r,\theta)$, were gathered synchronously using an eight-microphone array encircling a displaying individual's territory (Fig. 3). The bird was unrestricted in its choice of display sites and moved constantly around its territory. For each call location, there were eight different propagation paths, each with a unique $TL(f,r,\theta)$. There was a practical limit to the number of transmission loss curves that could be measured. In this first application of our method, we restricted our measures of the directional factor to calls that had been generated near the four sites where we had measured the transmission loss along all eight paths. We used acoustic localization to identify these vocalizations. This method enabled us to measure the beam pattern of individual call elements from individual calls without averaging across calls and without unrealistic assumptions about sound propagation.

Study site

We constructed acoustic radiation maps from recordings of three males displaying at a lek (lek 8) in Long Valley, Mono County, California, USA (37°40′N, 118°50′W) from 4 to 21 April 1997. This spanned the main period of display activity in this year. Lek 8, like most of the leks in this region, is located on a mostly flat alkali meadow surrounded by rolling hills of sagebrush. The vegetation on the meadow (*Carex* sp. and saltgrass) was sparse and low (as seen in Fig. 1).

Array recordings

We deployed recording arrays (Fig. 3) at two focal sites chosen to overlap 1–2 male display territories where female visits were common. In both these areas, we arranged the circular eight-point arrays using a Sokkia measuring system (DIO343) to measure angle and a tape measure for distance. We positioned the microphones at each point on this array at approximately female head height (approximately 20 cm) so that their diaphragms faced the center of the array. On one side of the array, 20 m from the center, we positioned a hide that served as an observation and recording station (see Appendix A for details of the acoustic recording system). We stretched alkali-resistant microphone cables from the microphones to the hide. Sage grouse avoid exposed cables so we buried the cables in shallow (4 cm) ditches. This array design minimized disturbance to the birds' movements and activities.

Using the Sokkia measuring system, we also assessed the relief of the encircled area (Fig. 3). This was accomplished by marking the distance from a fixed plane above the lek, determined by the height of the leveled survey scope, to the ground below. We measured this distance at 1 m intervals along the eight radial paths from the array center to each microphone location. From these data, we constructed topographic maps using MATLAB's 'contour' function, with the heights converted so that they were relative to the array's lowest point.

We made synchronous video recordings for all focal studies

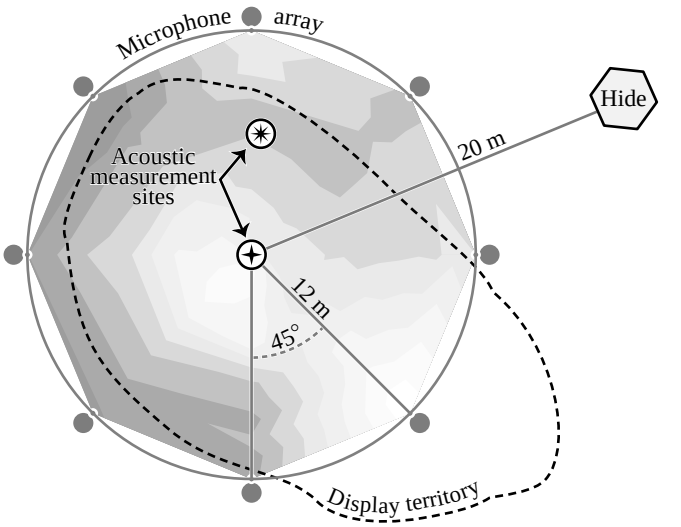

Fig. 3. Schematic drawing of the acoustic array deployment in relation to a male's display territory. An acoustic source was deployed for sound propagation measurement at two acoustic measurement sites, one of which was at the center of the array. The topography of the encircled area was measured when the array was deployed. A map of the relief is shown here with a contour interval of 10 cm.

using a Canon Hi-8mm ES2000 camera positioned in the hide approximately 0.75 m from the ground on a tripod. We synchronized the audio and video recordings by video-taping the running tape counter on the face of the audio recorder for a few seconds at the beginning of each recording session. Each day, we started recording as soon as there was sufficient light and continued until the males ceased their activity on the lek.

We designated two sites within each array as measurement positions: the center of the array and a position off center where the birds were seen calling. We measured transmission loss along each radial propagation path from these points as described in Appendices A and B. To minimize disturbance to the birds, we made these measurements in the birds' absence. Preliminary study showed that propagation properties are stable through the night and the display period (05:00–07:30 h), but change rapidly later in the morning (see Results and Fig. 4). These measurements were therefore made between 23:00 h and 03:30 h when the propagation effects are highly concurrent with those of the display period but the birds are absent.

Data acquisition

We digitally transferred all recordings to a Power Macintosh for analysis using an eight-track synchronous acquisition system (Digidesign ProTools v.4.1 with 888 I/O coupled to a TASCAM IF-88AE digital audio-interface unit). Using this software, we identified short sections of audio for detailed analysis, then created synchronized monaural files (22.05 kHz, wave format) for each track, which we transferred to MATLAB (MathWorks, 1998) for subsequent analyses.

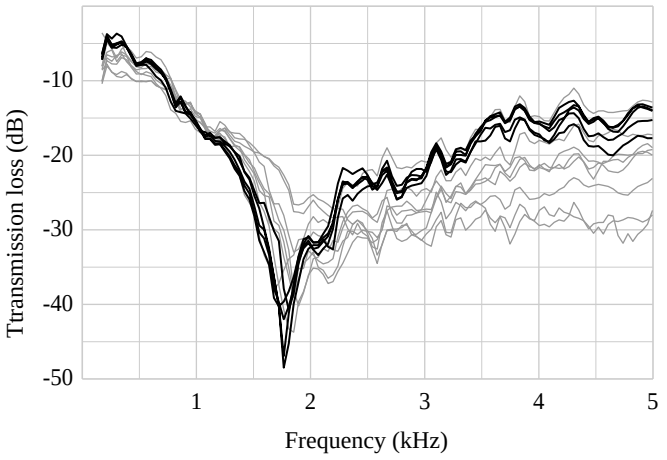

Fig. 4. Transmission loss functions for 12 measurements over the same 12 m stretch of the lek. Black lines show propagation during the period of display (05:00–07:30 h) and the period of calibration (23:30–03:30 h), while gray lines show the propagation at other times of day (08:00–23:00 h).

Acoustic localization

Our method for the mapping of acoustic radiation patterns required that vocalizations be produced near the designated measurement sites. We used acoustic localization to identify vocalizations produced in very close proximity to these calibrated sites ($\leqslant$1.5 m). Before localization, we preprocessed all signals with a highpass filter (second-order Butterworth with 200 Hz cut-off; MathWorks, 1998).

We employed a localization algorithm based on a least-squares best fit (Spiesberger and Fristrup, 1990) to equations that relate the sources' positions to the known locations of the microphones and the measured time delays in signal arrival between the microphones (Watkins and Schevill, 1971, 1972). We modified these equations in a number of ways. First, neglecting the small height variations of the lek surface, we reduced these equations to a two-dimensional case. Second, we employed the MATLAB function 'backslash' for the least-squares calculation of the over-determined set of linear equations (MathWorks, 1998). Third, the time delay estimates were taken from the peak location of the time-domain cross-correlation functions generated with the MATLAB function 'XCORR' (MathWorks, 1998; Shure and McClellan, 1997). Fourth, and most significantly, we calculated the final location estimate as the average location of eight semi-independent calculations made using each of the eight microphones as the designated reference. The algorithm requires the designation of a reference microphone, and previous users have designated a single receiver as this reference (Freitag and Tyack, 1993; Spiesberger and Fristrup, 1990; Watkins and Schevill, 1971, 1972). Our multi-reference algorithm increases the number of time delay estimates used in the calculation by a factor of four. In addition, only calls that showed a high correspondence between all eight location estimates were used in these analyses. We found that imperfections in the data (e.g. overlapping vocalizations, low signal/noise ratio) led to disparate estimates of location. This additional step allowed us to identify and purge these vocalizations from the data set.

Our system was well suited for acoustic localization using this algorithm. The method assumes that the speed of sound is known, that there is little wind and that receiver positions are accurately known (Spiesberger and Fristrup, 1990). Sound speed was calculated from air temperature measurements. Concurrent wind measurement allowed us to exclude data recorded during periods of wind in excess of 3 km h^{-1}. Receiver positions were definitely fixed and precisely known. Localization accuracy is high when the sound source is located near the microphone array (McGregor et al., 1997) and is best when the animal is completely encircled by receivers (Watkins and Schevill, 1971, 1972). Both were true of our experimental design. Also, the number of receivers, eight, far outnumbered the minimum (four) necessary to estimate the location unambiguously in two dimensions using this algorithm. In addition, the abrupt frequency and amplitude modulations of the sage grouse vocalization (Fig. 2) yielded sharp unambiguous peaks in the time-domain cross-correlation functions.

For each vocalization, the bird's location was combined with the orientation of the male relative to the receiver array to determine each receivers' value of θ for that call. The orientation could not be determined acoustically and was therefore estimated from the synchronous video recordings.

Beam pattern reconstruction

Band-averaged beam patterns, $b_{\mathrm{band}}(\theta)$, were then calculated for those calls that were generated at the measurement locations. The propagation delays, identified as part of the localization algorithm, were removed from the time series data in order to synchronize the signals. We then Fourier-transformed the data using a 128-point fast Fourier transform (with a zero-overlap Hanning window) and calculated the power spectral density, $|p_{\mathrm{r}}(f,r,\theta)|^2$. This, along with the measures of transmission loss, $TL(f,r,\theta)$, calculated as in Appendix B, were then substituted into equations 7 and 8 to yield the band-averaged beam pattern over a 5.8 ms time slice. The transmission loss corrections were truncated at the measurement-system noise floor, corresponding to TL=−45 dB.

The 5.8 ms duration of these time slices is arbitrary with respect to the vocalization. When we are interested in examining fluctuations in the beam pattern over short time scales, this time slice duration is useful. However, when the beam pattern is found to be fairly constant across an individual call component, it is more meaningful to map the beam patterns for the entire note of the acoustic display. Rather than just averaging the beam patterns of the individual time slices, we weight the time-averaged beam pattern so that the time slices that contain more acoustic energy contribute proportionally more to the measure of directionality. The

squared directional factor which is both band-averaged and time-averaged is:

$$H_{\text{band,note}}^2(\theta) = \frac{\frac{1}{n}\sum_{j=1}^{n}\Pi_{\text{band,j}}(\theta)}{MAX\left\{\frac{1}{n}\sum_{j=1}^{n}\Pi_{\text{band,j}}(\theta)\right\}}, \quad (10)$$

where n is the number of time slices over which the call component stretches; j is the time slice index and Π_{band} is the power in the frequency band defined in equation 7. Subsequently, the band-averaged beam pattern for that note is:

$$b_{\text{band,note}}(\theta) = 10\log H_{\text{band,note}}^2(\theta). \quad (11)$$

Beam pattern comparison

Maps of the beam patterns allow for qualitative comparisons of directionality. In addition, we can calculate numerical measures of these patterns which encapsulate the variation and allow quantitative comparisons. In this paper, we employ four such quantitative measures. These are: (1) angle of maximum lobe, θ_{max}, defined such that $b(\theta_{max})$=0 dB; (2) angle of the radiation pattern minimum, θ_{min}, defined such that $b(\theta_{min})$=*MIN*[$b(\theta)$]; (3) beam pattern range in dB, $|b(\theta_{max})-b(\theta_{min})|$; and (4) the directivity index, DI, also in dB. These values are presented as means ± standard deviations.

The directivity index (DI) measures the degree to which a radiation pattern is concentrated. This index compares the intensity of the maximum lobe of a beam pattern with the intensity of a uniform source radiating the same total power output. In this way, the DI incorporates aspects of the radiation field off the maximum lobe whereas beam width measures do not. Derivations of DI are available elsewhere for three-dimensional radiation patterns (e.g. Kinsler et al., 1982). In Appendix C, we derive an analogous measure for radiation patterns resolved only in a single plane.

Results

Environmental acoustics

Transmission loss fluctuated with time of day but was stable from 22:30 to 07:30 h (Fig. 4). Therefore, late-night measurements made within a bird's territory while the animal was away were highly concurrent with propagation during the period of display. Below 1.2 kHz, these transmission loss measurements were extremely consistent, differing in value by a mean of 1.1±0.5 dB (N=5). The higher frequencies, 1.2–5.0 kHz, show more variation, 3.7±1.8 dB (N=5), across the time window of calibration and bird display. Because of this variation in the transmission loss curves over time, we estimate our error of measurement for beam pattern mapping to be ±2 dB below 1200 Hz and ±4 dB above 1200 Hz.

The transmission loss curves for sound propagation over the different paths of the lek (Fig. 5) show many similarities but also important differences. Measurements made from the center of each array are easiest to compare since the path lengths are equal (Fig. 5C,D). In both arrays, transmission loss curves for each path are highly concordant below 500 Hz. At these low frequencies, sound propagation was reliable across paths and less acoustic pressure was lost in transmission than in free-field spherical spreading. The low-frequency components of the sage grouse display (coos and pop 2) have most of their energy in this well-propagated frequency range (Fig. 2). Therefore, these components of the strut display must propagate reliably across fairly long distances.

In contrast, the higher-frequency whistle spans a less reliable frequency band from 0.6 to 3.2 kHz (Fig. 2). Sound in this range propagated far less effectively than free-field spherical spreading. Also in this frequency range we find a deep propagation minimum (notch) in the transmission loss curves of all paths. The exact position of this notch is variable between paths but is always between 1 and 2 kHz. Even outside the path-specific propagation notch, there are 10–15 dB differences in transmission loss between the paths. Long-distance communication in this frequency range is very unreliable, suggesting that the whistle component of the call might be an exclusively close-range component of sage grouse communication. Shorter paths show shallower notches and a concomitant decrease in the frequency-dependence of propagation (Fig. 5D,E).

The major features of our transmission loss curves (Figs 4, 5) are consistent with the measured curves and models of previous acoustic studies of sound propagation close to the ground (Embleton, 1996; Embleton et al., 1976, 1983). These major features include (1) low levels of loss for the low frequencies, (2) a stop-band notch in the intermediate frequencies due to interference between the direct and reflected paths and (3) lower levels of loss again for the higher frequencies where the reflected paths are less coherent. These features are expected for propagation near most surfaces.

There is, however, much heterogeneity between the transmission loss curves, even those with identical path lengths (Fig. 5C,D). Differences between these curves reveal propagation effects that arose from differences in topography (Fig. 5A,B) and soil composition. No extant acoustic model sufficiently explains the heterogeneity in the propagation curves that we have presented here. However, using our method, we were still able to reconstruct beam patterns for calls produced at sites where we had made empirical measures of the transmission loss. All these sites and their associated transmission loss curves are shown in Fig. 5.

Acoustic localization

We identified 39 vocalizations produced within 1.5 m of our calibration sites: 30 vocalizations from male A, seven from male B and two from male C. Although this sample is skewed towards a single individual, the range of directionality exhibited by male A subsumes the range of values exhibited by the other two males. Therefore, we consider each vocalization to be independent for statistical analysis. Where

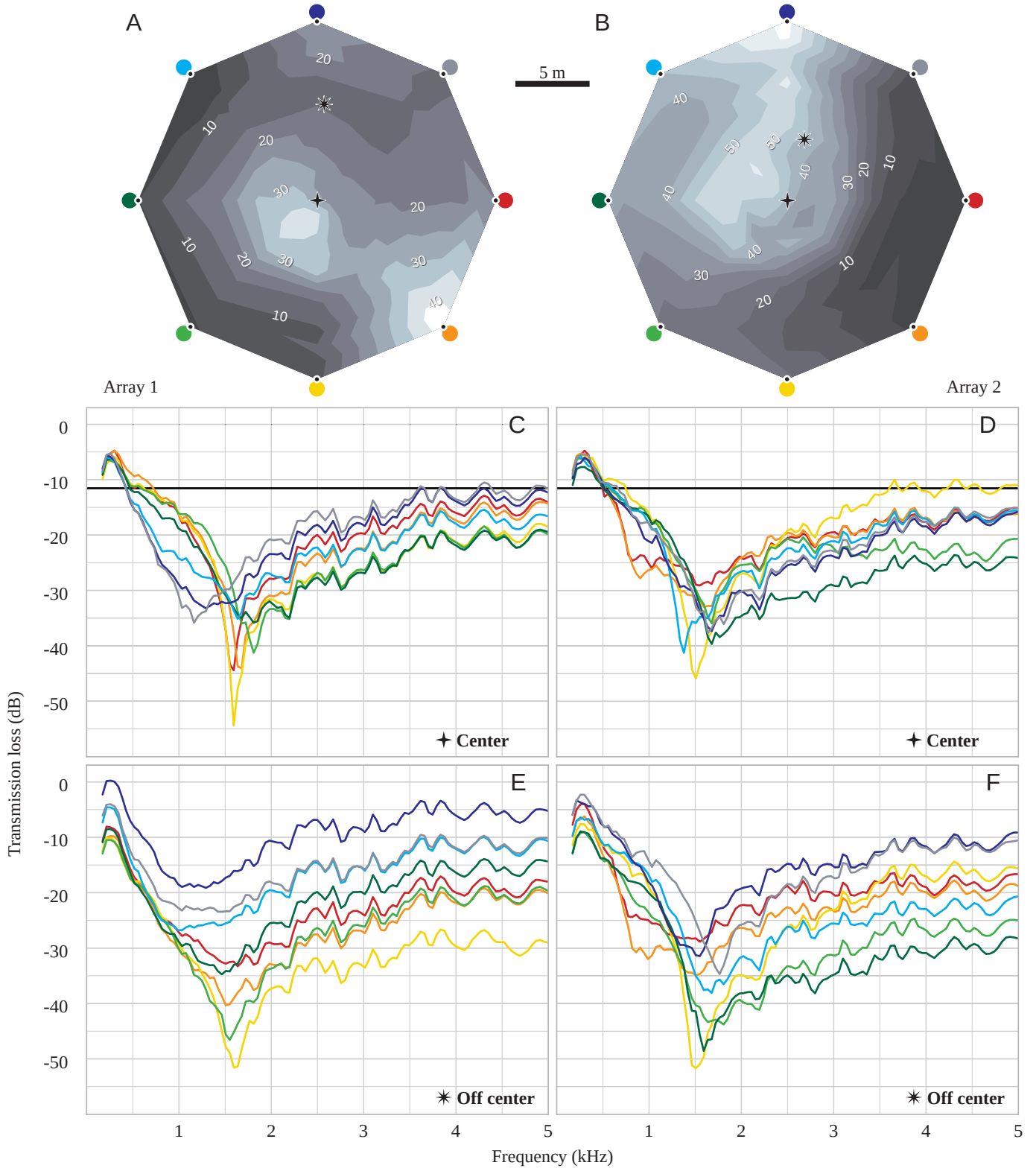

Fig. 5. Transmission loss curves for all propagation paths used for the reconstruction of acoustic radiation patterns and topographic maps of each recording array. (A,B) The maps of each array show topographic features (with elevation in cm) in relation to the location of the acoustic measurement sites and the microphones. The microphones are color-coded, corresponding to the line color of the transmission loss curve from the measurement site to that microphone. (C,D) Transmission loss for propagation paths from the center of the array to each of the microphones. The solid black horizontal line shows the level of transmission loss expected from spherical spreading alone. (E,F) Transmission loss for propagation paths from the off-center measurement site to each of the microphones. Since the propagation path lengths are unequal, the transmission loss expected due to spherical spreading alone is different for each path. For simplicity, these values are not shown.

appropriate, we also present directionality measures for each individual. In our subsequent studies, we will use an omnidirectional speaker that allows us to calibrate more sites within each array and thereby achieve sample sizes sufficient for comparisons between males.

Beam patterns

We found that the acoustic component of the sage grouse strut display is directional. This directionality showed high between-note variability in all measured vocalizations. However, we found that the coos and pops showed high within-note stability in their beam patterns. These notes, therefore, were best examined by calculating time-averaged beam patterns, $b_{\mathrm{band,note}}(\theta)$. In contrast, the beam patterns of the frequency-modulated whistles varied significantly in time and consequently were examined as a series of discrete time slices, $b_{\mathrm{band}}(\theta)$.

The coo notes had directional beam patterns (Table 1) which were consistent between the two coos of a single call but variable between vocalizations (Fig. 6). The beam patterns of the coos tended to be loudest to the front and quietest at the sides, with a variable amount of energy radiated behind the displaying bird. The orientations of the major lobes of the coo beam patterns were variable with respect to the anterior–posterior axis of the birds. In many vocalizations, the maximum lobe was rotated by up to 45 ° to either side of the bird, and in some examples the posterior lobe was actually slightly louder than the anterior lobe. Fig. 7 illustrates these trends as histograms of the maximum and minimum points on each beam pattern, θ_{max} and θ_{min}. These maxima and minima had significantly non-random angular distributions (Table 2).

The two pops showed markedly different beam patterns from the coos and from each other. Pop 1 was strongly directional (Table 1) but the angular distribution of the beam pattern maxima and minima was not distinguishable from random (Rayleigh test: combined data set, N=39, P>0.1). Pop 2 was much less directional (Table 1). The beam pattern range for many vocalizations fell below the noise floor of our technique, 4 dB in this frequency band. However, when we restricted our examination of the directionality to those pop 2 notes with a beam pattern range greater than the potential measurement error, we found that, when the beam pattern was significantly directional, this pop tended to be louder in front of the bird and quieter behind (Table 2).

During the duration of the whistle, both the dominant frequency and the air-sac geometry change extensively. This variation should be accompanied by fluctuations in the directionality of acoustic radiation. Such variability was seen in all whistles (Fig. 8). Despite this variability, all whistles showed a deep anterior null in the beam pattern. This null was not present for the entire whistle but was always present for at least part of it. In contrast to the beam patterns of the coo and pop notes described above, the modal positions of the whistles' beam pattern minima, mode[θ_{min}], were typically in front of the strutting bird (Fig. 9; Table 2). In addition, the modal maxima, mode[θ_{max}], of the whistles were never in front of the bird but were oriented to either side or behind. Thus, the angular distribution of the whistles' modal maxima and minima are the inverse of the coos' distributions. On average,

Table 1. *Directionality of the coo and pop notes of the sage grouse strut display*

Male	N	$b_{\mathrm{band,\,note}}(\theta)$	Coo 1	Coo 2	Pop 1	Pop 2
A	30	Range (dB)	8.5±2.3	9.7±2.3	9.6±3.8	5.0±1.4
		DI (dB)	3.3±1.0	3.7±0.9	3.8±1.4	2.5±0.7
B	7	Range (dB)	8.6±2.6	7.6±1.6	11.4±3.3	6.2±1.5
		DI (dB)	3.4±1.5	3.2±1.3	4.3±1.0	2.5±0.8
C	2	Range (dB)	9.7±2.7	9.8±1.4	5.3±0.0	4.2±0.1
		DI (dB)	2.8±0.2	2.8±0.2	3.1±0.0	1.8±0.1
All	39	Range (dB)	8.6±2.4	9.4±2.3	9.7±3.8	5.2±1.4
		DI (dB)	3.3±1.1	3.6±1.0	3.8±1.3	2.5±0.7

The mean and standard deviation of two measures of directionality are shown for each individual and for the entire sample of vocalizations.

The top value is the range of the measured values of the beam patterns. The bottom value is the directivity index (DI) of those patterns. A uniform sound field has a DI of 0 dB and a dipole has a DI of 3.01 dB (see Appendix C).

$b_{\mathrm{band,\,note}}(\theta)$, time- and band-averaged beam pattern.

Table 2. *Results of Rayleigh tests on the angular distribution of the beam patterns' maxima and minima, θ_{max} and θ_{min}*

Call note	Beam pattern measure	All males	Male A	Male B
Coo 1	θ_{max}, forward	z=7.81	z=5.34	z=2.86
		N=39	N=30	N=7
		P<0.001	P<0.005	P<0.1 (NS)
	θ_{min}, sideways	z=7.38	z=6.01	z=2.03
		N=39	N=30	N=7
		P<0.001	P<0.002	P<0.2 (NS)
Coo 2	θ_{max}, forward	z=19.02	z=13.75	z=3.56
		N=39	N=30	N=7
		P<0.001	P<0.001	P<0.05
	θ_{min}, sideways	z=12.17	z=9.44	z=4.56
		N=39	N=30	N=7
		P<0.001	P<0.001	P<0.01
Pop 2	θ_{max}, forward	z=9.19	z=5.38	z=2.94
		N=29	N=21	N=6
		P<0.001	P<0.005	P<0.1 (NS)
	θ_{min}, behind	z=9.25	z=8.82	z=3.84
		N=29	N=21	N=6
		P<0.001	P<0.001	P<0.02
Whistle	mode[θ_{max}], sideways	z=4.70	z=4.33	z=4.43
		N=39	N=30	N=7
		P<0.01	P<0.02	P<0.01
	mode[θ_{min}], forward	z=11.06	z=6.73	z=3.36
		N=39	N=30	N=7
		P<0.001	P<0.001	P<0.05

No tests were conducted for male C because the sample size was insufficient.

NS, not significant.

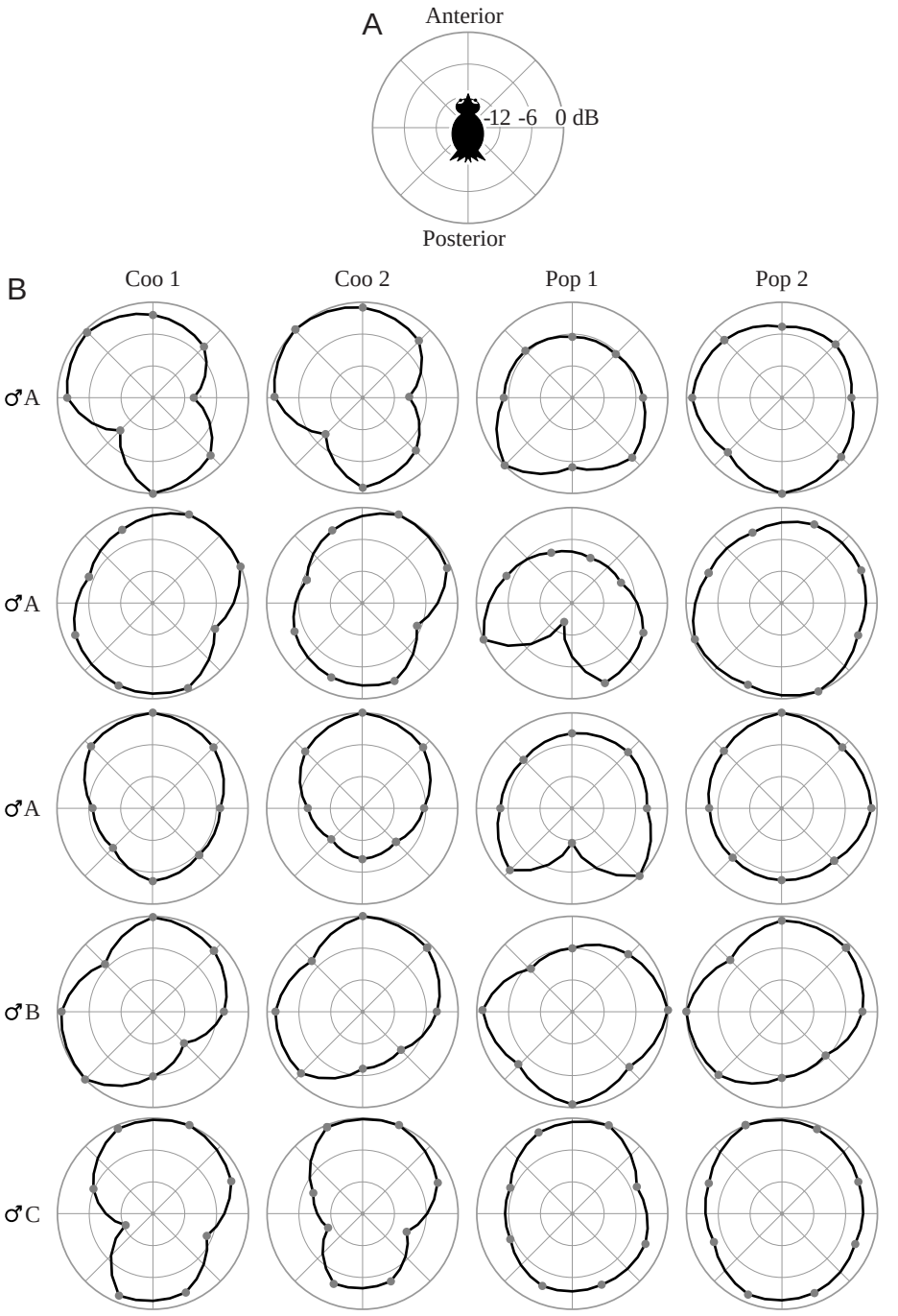

Fig. 6. Acoustic beam patterns, $b_{band,note}(\theta)$, for the coos and pops. (A) Polar diagram showing the format of all acoustic radiation plots used here. Viewed from above, the birds are standing at the center facing upwards. Divisions are 6 dB. Here, the dynamic range represented is 18 dB. (B) Beam patterns of five representative strut displays. The first three rows show the range of patterns observed from male A. The last two rows show one strut from each of the other two focal males (males B and C). The frequency bands used in the average were 300–600 Hz for coo 1, coo 2 and pop 2 and 600–1200 Hz for pop 1.

the whistle was highly directional and extremely variable (Table 3). At its most directional time slice, the average whistle was 22.9±3.4 dB less intense in front of the calling bird than it was at the sides (Table 3).

Discussion

The results described above show that sage grouse strut displays have strikingly directional patterns of acoustic radiation. Here, we compare these directional patterns with the patterns observed in other vertebrates and show that the sage grouse radiates sound in a fashion that is fundamentally different from that for any previously measured vertebrate (see Gerhardt, 1998, and below for review). To measure these patterns and map them accurately, we had to develop a new method for the measurement of acoustic directionality in the field. We start our discussion by explaining the major novelties and advantages of our method that allowed us to make these discoveries.

Methodological conclusions

There are two features of our method for measuring acoustic emission patterns that are advantageous relative to previous methods used in both laboratory and field studies:

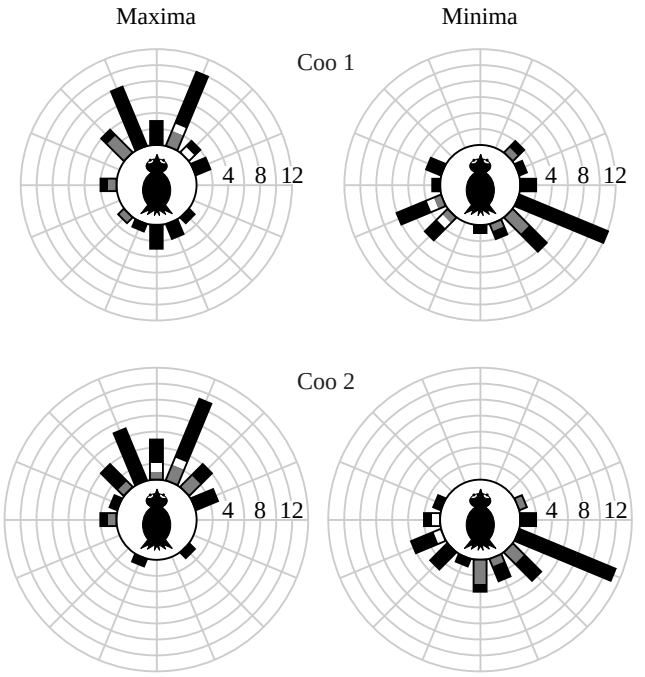

Fig. 7. Polar histograms showing the orientation of the beam patterns' major features relative to the anterior–posterior axis of the birds for coo 1 (top) and coo 2 (bottom). These frequency distributions show beam pattern maxima (left), θ_{max}, and minima (right), θ_{min}, for all 39 measured vocalizations. The contribution of each focal male is indicated by the density of the cell in each histogram bar; black is male A, gray is male B and white is male C.

Table 3. *Directionality of the frequency-modulated whistle of the sage grouse strut display*

Male	*N*	$b_{band}(\theta)$	Mean	Maximum	Minimum
A	30	Range (dB)	13.6±2.1	22.8±3.6	6.3±1.7
		DI (dB)	4.4±0.6	6.7±0.8	2.2±0.5
B	7	Range (dB)	16.1±2.1	23.6±3.2	8.5±1.2
		DI (dB)	4.6±0.3	6.8±0.5	2.7±0.4
C	2	Range (dB)	12.0±0.2	22.7±0.9	3.6±0.2
		DI (dB)	3.8±0.1	6.7±0.3	1.6±0.2
All	39	Range (dB)	14.0±2.3	22.9±3.4	6.5±1.9
		DI (dB)	4.4±0.5	6.7±0.7	2.3±0.6

The mean and standard deviation of two measures of directionality are shown for each individual and for the entire sample of vocalizations.

The top value is the range of the measured values of the beam patterns. The bottom value is the directivity index (DI) of those patterns.

$b_{band}(\theta)$, band-averaged beam pattern.

(1) synchronous recordings from multiple angles around the focal individual, (2) explicit measurement of environmental effects on propagation. Here, we examine the specific advantages associated with each of these features.

Advantages of synchronous recordings

Previous studies have made detailed beam pattern maps using two microphones by repeatedly repositioning a single receiver at various angles while another remains in a fixed position to correct for fluctuations in overall amplitude. This asynchronous, two-microphone method allows for fine spatial resolution in the mapping of acoustic fields and has been used to reconstruct some very complicated radiation patterns (Au et al., 1995; Bennet-Clark, 1987; Forrest, 1991; Hartley and Suthers, 1987, 1989, 1990; Hunter et al., 1986; Larsen and Dabelsteen, 1990). The only limit to the spatial resolution is the number of measurement sites chosen by the researcher. However, this method can only be used when the focal animal's position is fixed by behavior or design and the same vocalization can be coaxed or induced for repeated measures. In addition, using asynchronous measures to reconstruct radiation patterns assumes that beam patterns remain constant between vocalizations of the same type. Our synchronous recording technique allowed us to test this assumption in sage grouse. Our results show that the beam patterns for each call note vary between vocalizations. Therefore, this assumption may be inappropriate for some organisms, and synchronous recording is therefore preferred (Gerhardt, 1998). The trade-off associated with synchronous recording is that the spatial resolution of radiation maps is limited by the number of receivers deployed. This number has practical limitations, especially in the field. However, our eight-microphone design was sufficient to describe the major features of the radiation patterns produced by sage grouse.

Advantages of explicit environmental measures

Laboratory study of acoustic emission fields has one principal advantage over our method: a controlled environment. Anechoic recording chambers obviate detailed environmental calibration since the measures of the acoustic field are direct measures of the emission field. For many organisms, laboratory study is impossible or impractical and measures must be made in the field. Field study also allows for the measurement of acoustic directionality in the context of natural display behavior. Field studies must account for the complexities of propagation in natural environments. Previous field studies of acoustic directionality have dealt with the environment by either assuming or demonstrating (a) that sound propagation is not frequency-dependent over the measurement distance and (b) that environmental effects are homogeneous across the measurement paths. These simplifications allow the treatment of field measurements as if they were conducted in an anechoic chamber and thus require no explicit corrections for propagation effects. These simplifications may be appropriate (a) when the measurement propagation paths are very short, (b) when there are no nearby surface boundaries, and (c) when all paths are free from heterogeneous features. To make measurements on unrestrained and mobile sage grouse in the wild, our method used longer measurement distances over a heterogeneous surface boundary. Therefore, neither simplification was appropriate. Instead, we measured the precise transmission loss curve for each measurement path

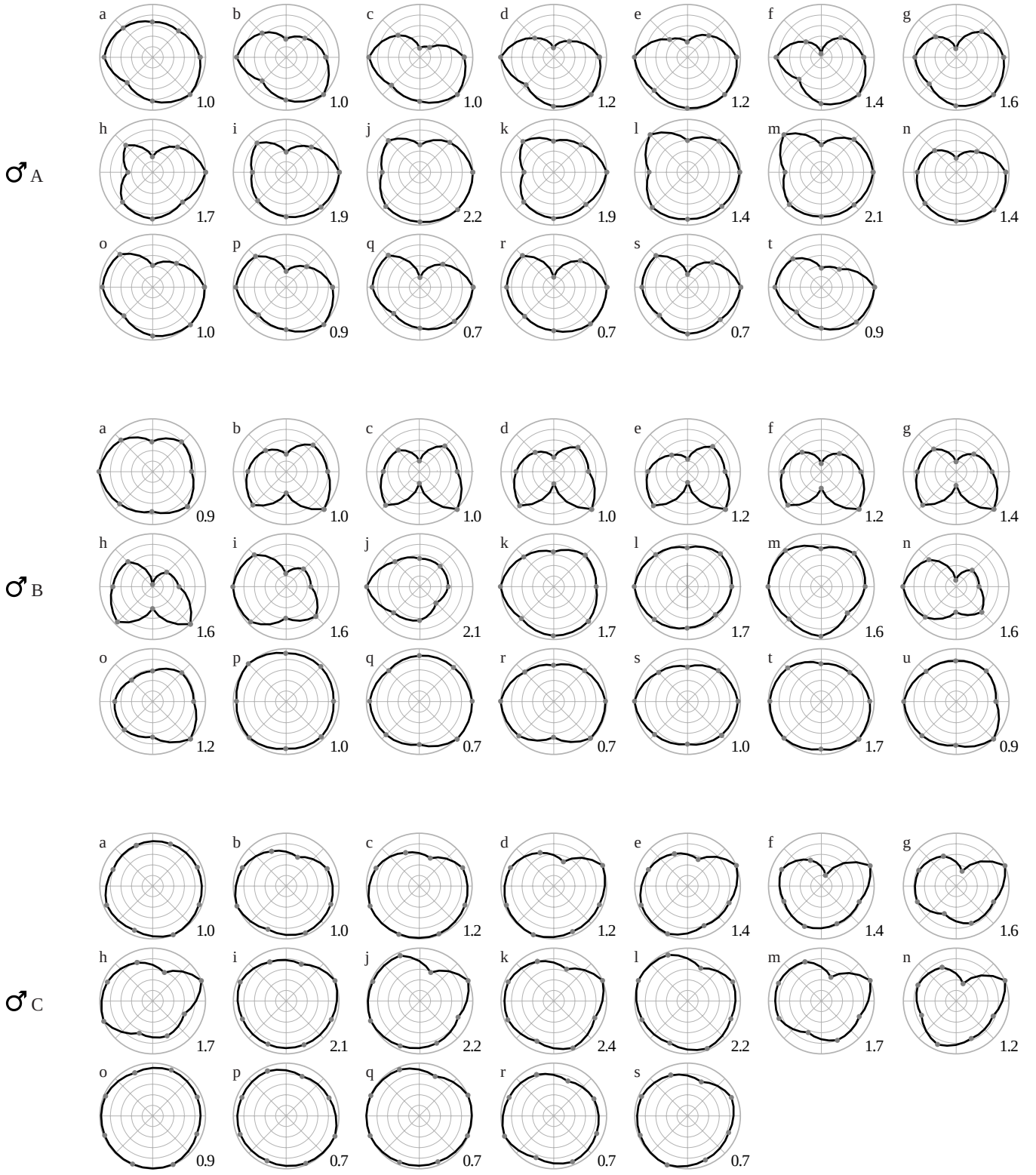

Fig. 8. Time-varying beam patterns, $b_{band}(\theta)$, for the whistle component of the strut display. The format is the same as in Fig. 6 except that the dynamic range of these plots is 30 dB. Each plot represents a time slice of 5.8 ms with no overlap. Time reads from left to right and from top to bottom, signified by the letters a–u. The value at the bottom right of each polar plot is the dominant frequency (kHz) for that time slice. One whistle from each focal bird is shown.

and explicitly corrected for propagation heterogeneity in frequency and space. In this way, our method makes acoustic-directionality research possible in a wider variety of organisms and environments.

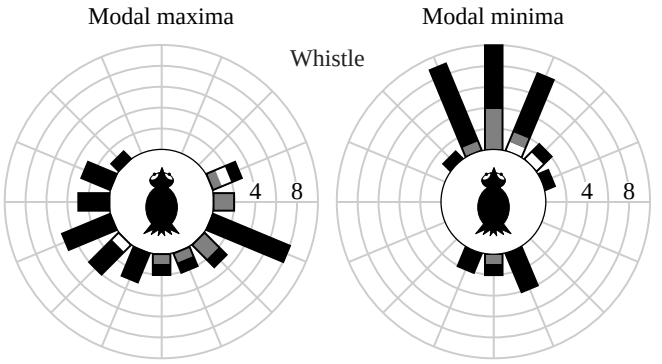

Fig. 9. Polar histograms showing the orientation of the beam patterns' major features relative to the anterior–posterior axis of the birds for the whistle. These frequency distributions show beam pattern modal maxima (left), mode[θ_{max}], and modal minima (right), mode[θ_{min}], for all 39 measured vocalizations. The contribution to the data set of each focal male is indicated by the density of the cell in each histogram bar; black is male A, gray is male B and white is male C.

Bioacoustic conclusions

Our measurements showed that sage grouse strut displays have markedly directional acoustic beam patterns. Although the directionality of these patterns varied both within a vocalization and between calls, clear patterns emerged. First, the coos were always intense in front of the animal and sometimes intense behind as well. The coos were least intense to either side. This maximal lobe rotated up to 45 ° to either side between vocalizations. The whistles showed a distinctly different beam pattern. While variable across the length of the note, the principal beam pattern that dominated the radiation of the whistle was laterally bilobate with a strong anterior null in the beam pattern. Pop 1 was strongly directional but highly variable in its orientation, whereas pop 2 had a much lower magnitude of directionality but was fairly stable in its directional pattern.

Comparisons with the directionality of other vertebrate vocalizations

The acoustic radiation patterns of a number of other vertebrate vocalizations have been measured and they conform to a general theme. Directional vertebrate vocalizations are bilaterally symmetrical with their maximal radiation point anterior to their site of acoustic radiation (mouth, nares or vocal sac). This is consistent with models of single-site acoustic radiation. The degree to which these fields are directional varies from a narrow beam to nearly or completely omnidirectional. The most directional vocalizations, with approximately 20–36 dB in beam pattern range, are the echolocation pulses of bats and of toothed whales (Au et al., 1995; Fuzessery et al., 1992; Hartley and Suthers, 1987, 1989, 1990; Pilleri et al., 1976; Purves and Pilleri, 1983; Schnitzler and Henson, 1980; Wotton et al., 1997). Few of the above studies resolved these patterns beyond the forward-facing 180 °, so these range values are estimates and it would be inappropriate to estimate DIs. Intermediate directionality, with beam pattern ranges of 6–15 dB and DI between 2.0 and 3.5 depending on frequency, has been found in human speech and blackbird vocalizations (Flanagan, 1972; Larsen and Dabelsteen, 1990). Anuran calls are at the low end; the most directional of the measured frog calls has a beam pattern which ranges 6 dB from front to back (DI≈1.5) (Gerhardt, 1975). Most frogs vocalizations are much less directional and some have been found to exhibit a nearly omnidirectional pattern, DI≈0 (Gerhardt, 1975; Passmore, 1981; Prestwich et al., 1989).

To our knowledge, there are only two previously reported minor exceptions to the vertebrate theme that vocalizations are loudest in front and quieter behind. One species of toad, *Bufo americanus*, radiates sound in two equally intense lobes 180 ° apart, one in front and one behind, separated by a notch of approximately 3–4 dB (Gerhardt, 1975). The fairly shallow lateral null in this pattern is an interesting deviation from the standard vertebrate pattern and remains unexplained. Also, the call of the African frog *Cacosternum boettgeri* was reported to be 1–1.5 dB louder directly posterior (Passmore, 1981). This effect was extremely small, within the range of likely measurement error for working in the field. In addition, since this study did not account for propagation effects, it is possible that the skew was environmentally induced.

Portions of the sage grouse whistle show the greatest directionality of any strictly communicative vertebrate signal so far measured. Only vocalizations used for echolocation are known to be more directional. The sage grouse coos and pop 1 show the level of directionality commonly found in the communication signals of larger vertebrates, while pop 2 is more similar to the omnidirectional sounds of frogs. We expected that lower-frequency sounds, those with large wavelength-to-body size ratios, would be less directional than higher-frequency sounds (Bradbury and Vehrencamp, 1998; Prestwich, 1994). This held generally true in sage grouse since the whistle contains energy principally in wavelengths shorter than those of the less-directional coo and pop notes. However, despite having a similar spectral make-up, pop 2 is markedly less directional than the two coos. Also, the lower frequencies of the whistle, 500–1400 Hz, often exhibited the deepest anterior nulls and the strongest directionality. Therefore, we propose that the rapid movement of the esophageal air sac or associated structures is responsible for much of this between-note variation in magnitude of directionality.

While the magnitude of the directionality is not completely unprecedented, the shape of the beam patterns of the sage grouse strut is unlike any previously seen in vertebrates. The two most surprising results are the deep anterior null in the radiation pattern of the whistle and the bilateral asymmetry and variable direction of the peak in the radiation pattern of the coos and pop 1. Previous attempts to understand the patterns generated by vertebrate vocalization have used simple acoustic models of single-source radiation to arrive at a realistic estimate of radiation mechanisms. A model of the vocal apparatus as a vibrating piston suspended in a baffle has adequately explained the basic patterns observed in birds, bats,

cetaceans and humans (Flanagan, 1972; Hartley and Suthers, 1989, 1990; Hunter et al., 1986; Larsen and Dabelsteen, 1990; Mogensen and Møhl, 1979; Pilleri, 1990; Stevens, 1997; Strother and Mogus, 1970). Alternative models of single-site radiation have come closer to explaining the smaller side lobes in the acoustic field of bats (Hartley and Suthers, 1989, 1990). One dual-site radiation model argued that emission through a paired structure could lead to an increase in directionality for bats that call through their noses (Möhres, 1967; Sokolov and Makarov, 1971).

The beam patterns seen in the sage grouse do not fit those predicted by any of these models. The shape of the beam patterns for the coos and pops superficially resemble some of these patterns. However, since all the potential radiation sites (mouth and air sacs) face forwards for the duration of the vocalization, none of these models can explain the variability in the location of the peak or the intensity of the rearward-facing lobe. Furthermore, none of the models can explain the anterior null and lateral projection of the whistle component. Because of this lack of congruence with existing models, we suggest that the sound emission mechanism of the sage grouse is unlike that of any other vertebrate so far examined.

Directionality, display posture and the study of mate choice

Even directionality as low as 3–6 dB is likely to be behaviorally relevant because, given spherical spreading, this translates to a 40–100 % greater distance of propagation in the direction of the maximum lobe before the signal is lost. Directionality is a defining component of an acoustic signal's active space, although it is often overlooked (e.g. Brenowitz, 1982). When a sender knows (or can estimate) the location of its intended receiver, the signaler can reduce the cost of eavesdropping by predators and competitors by turning so that the peak of its beam pattern corresponds to the position of the receiver. The signaler can then produce just enough acoustic power to signal effectively to that individual (Klump and Shalter, 1984; Larsen and Dabelsteen, 1990). In addition, when competitors have overlapping signals, the sender can combine display orientation with a more powerful vocalization to decrease acoustic interference from its competitors and maximize the probability of response by the receiver. If the receiver can perceive the vocalization's directionality, then appropriate posture might also help to specify the intended recipient of the signal (McGregor and Krebs, 1984; Richards, 1981). In these ways, directional patterns of acoustic radiation can strongly influence the choice of display posture, allowing for more effective or efficient communication to receivers of known location. When the intended receiver's position is unknown, however, directional display can be a liability necessitating continual modification of display posture to maximize the probability of reception (Forrest, 1991). In situations like this, an omnidirectional vocalization may be favored. The directionality of vertebrate vocalizations is likely to be tuned to the social and environmental context of the display, and display posture is likely to reflect the degree and nature of that directionality.

Sage grouse males do not face females head on. Early observers of the mating display of the male sage grouse noticed that, although the display was dramatic, the efforts seemed to be unrelated to the locations of potential female mates. Simon (1940, p. 470) wrote that the males, 'seemed disinterested in the hens...[and] in strutting paid very little attention to [them]'. Indeed, while males rotate to different directions for successive calls, they rarely face a female head on (J. W. Bradbury and M. S. Dantzker, personal observation). Females turn with the male to help maintain an oblique angle between them (Wiley, 1973a). It is this indirect approach that fooled Simon (1940) into his incorrect inference that the sage cock was not in 'actual pursuit' of hens. We now know that lekking sage grouse are under intense sexual selection driven by female choice (Gibson and Bradbury, 1985; Hartzler, 1972; Hjorth, 1970; Lumsden, 1968; Patterson, 1952; Scott, 1942; Wiley, 1973b). The results of this study suggest that, despite maintaining an oblique orientation, male sage grouse might still reach females with the loudest portion of his acoustic signal. Beyond this, however, these data do not reveal the adaptive significance of the unusual radiation patterns we have described. While it is possible that these beam patterns evolved under direct selection, it is also possible that the patterns are an epiphenomenon of selection for loud or impulsive sounds. Alternatively, the patterns of acoustic radiation might have evolved to improve the efficacy of an already lateralized display that evolved first for other reasons.

Investigations of female sage grouse mate-choice have identified a number of spectral and temporal aspects of the strut display that are correlated with mating success (Gibson, 1996; Gibson and Bradbury, 1985; Gibson et al., 1991). While amplitude is likely to be an important determinant of mate attraction (Forrest and Raspet, 1994), these studies could not examine signal intensity since field measurements were not repeatable (J. W. Bradbury, personal observation). The results of the present study suggest that the unusual and variable beam patterns of the sage grouse display combined with the leks' heterogeneous transmission loss blocked these previous efforts from accurately measuring signal amplitude. These same factors, directionality and heterogeneous transmission loss, also stymie efforts to measure the amplitude of other species' acoustic displays (Gerhardt, 1998). Techniques such as the one we have described here facilitate the study of acoustic amplitude in the field and thereby allow more thorough investigation into the importance of amplitude and directionality in signal evolution.

Appendices

Appendix A: calibration of the acoustic system

The acoustic system, described below, had its own characteristic acoustic properties. These properties had to be identified and quantified before the system could be used to measure the transmission properties of the lek and the radiation pattern of the sage grouse. This Appendix outlines how this was accomplished. In what follows, we will assume that all

time variables have been Fourier-transformed so that we are dealing with the steady-state response of the system.

The acoustic system consisted of source and receiver components. The sound source was a Kudelski powered speaker driven by a Stanford Research DS340 signal generator. A single receiver channel consisted of an Audiotechnica MB1000L microphone coupled to a custom-built amplifier through an impedance-matching transformer. The output from the amplifier was recorded on a TASCAM DA88 digital recorder, which provides 96 dB of dynamic range from 10 Hz to 22.5 kHz.

The source sound pressure field measured 1 m from the front of the source can be related to the signal generator voltage by:

$$p_s(f) = \alpha_s(f) V_g(f), \tag{A1}$$

where $V_g(f)$ is the voltage supplied by the generator and $\alpha_s(f)$ is a frequency-dependent constant, which depends on the source and has units of $\mathrm{Pa\,V^{-1}}$. Similarly, the voltage at the output of the amplifier can be expressed as:

$$V_r(f) = \frac{p_r(f)}{\alpha_r}, \tag{A2}$$

where $p_r(f)$is the sound pressure at the microphone and α_r is a frequency-independent constant for the microphone/amplifier pair, which also has units of $\mathrm{Pa\,V^{-1}}$. The frequency-independent response of the Audiotechnica microphone and custom-built amplifier was verified by comparison of the response with a calibrated APO microphone.

The third expression we require relates the acoustic field radiated by the source to the field that arrives at the microphone. For the acoustic system calibration, the source was positioned close to the microphone and away from the ground to prevent interference from multi-path arrivals. In this case, the relationship between p_s and p_r follows a spherical spreading law:

$$p_r = \frac{p_s}{r}, \tag{A3}$$

where r is the separation between the speaker and microphone. This relationship was tested and found to hold true by measuring the source spreading loss at three ranges, verifying that the calibration measurements were not made in the near field of the source and were free from multi-path effects.

To characterize the acoustic system, it was necessary to measure α_s and α_r. In our later calculations, these two constants will always appear as a dimensionless ratio, and so it is sufficient to measure α_r/α_s. Combining equations A1, A2 and A3, we have:

$$\frac{\alpha_r}{\alpha_s} = \frac{V_g}{V_r r}, \tag{A4}$$

where the explicit dependence on frequency has been dropped. The ratio defined in equation A4 was determined by measuring r and the variables V_r and V_g across a frequency band of 200 Hz to 5 kHz.

Appendix B: measurement of transmission loss across the lek

Acoustic transmissions close to the ground are characterized by frequency-dependent structure in the transmission loss caused by interference between airborne and ground-reflected arrivals. Absorption and refraction due to sound speed profiles in the air are not expected to be important over the short ranges and low frequencies of interest here (Piercy and Embelton, 1977). The ground-induced interference structure depends sensitively on the composition of the ground (Embleton et al., 1983) and ground relief. As the ground relief varied considerably along the transmission paths studied, the transmission loss along each path needed to be measured.

The subject of acoustic transmissions over ground is a subject area in its own right, and a full discussion of the phenomenon lies beyond the scope of the present paper. The interested reader is referred to the work of Embleton et al. (1976, 1983) and recent reviews by Embleton (1996) and Forrest (1994).

The transmission loss across a given stretch of the lek is defined by:

$$TL(f,r) = \frac{p_r(f,r)}{p_s(f)}, \tag{B1}$$

where $p_r(f,r)$ is the sound field pressure at the observation point as a function of range from the source, r, and frequency, f, and $p_s(f)$ is the free-space source sound pressure field measured 1 m in front of the source. Substituting equations A1 and A2 into equation B1, we obtain:

$$TL(f,r) = \frac{\alpha_r}{\alpha_s(f)} \frac{V_r(f,r)}{V_g(f)}, \tag{B2}$$

where the constants α_r and α_s depend on the acoustic measurement system (see Appendix A), V_r is the voltage measured at the microphone and V_g is the voltage used to drive the source. Since the ratio $\alpha_r/\alpha_s(f)$ is known, the transmission loss can be measured by measuring $V_r(r,f)$ and $V_g(f)$.

The actual measurement methodology for a given stretch of the lek was as follows. The measurement system was composed of the instruments described in Appendix A with the exception of the Stanford Research signal generator, which was replaced by a recording of the signal generator output. The Kudelski speaker was placed within the microphone array with its center 25 cm above the ground using a leveled stand and driven with a sinusoidal chirp linearly modulated with a triangle-wave from 200 Hz to 5 kHz. A complete chirp took 10 s to complete, providing sufficient time at any given frequency to allow for all multi-path arrivals. For each measurement path, we recorded four complete chirps of both the source excitation voltage and the microphone response voltage. At each acoustic measurement site, we repeated this measurement procedure eight times, rotating the speaker each time so that the speaker faced directly towards each microphone in the recording array. Like most loudspeakers, the Kudelski speaker is directional; however, the rotation of the speaker allowed us to calibrate our system with an effectively omni-directional source.

The most straightforward way to determine the ratio of voltages that appears in equation B2 would be to compute the ratio of the Fourier-transformed time series. However, in practice, it was found that this methodology was too sensitive to contamination from sources of ambient noise, which included wind and biological sources. Therefore, we employed a noise-reduction algorithm to improve the ratio estimates. The algorithm consisted of the following. For each transmission path, 30 s or three complete chirps of source excitation and microphone response voltages were digitally transferred from the tape to a computer. The digital data streams were pre-processed by cross-correlating the source and microphone voltages to determine the time delay in the transit of the airborne signal between the source and microphone. This time delay was then backed out of the microphone recording to synchronize the source and microphone time series so that the dominant frequency, f_j, within a given segment of source and microphone data was the same. The voltage ratio at f_j was then determined by taking the ratio of the spectral levels at f_j while ignoring all other spectral components. Thus, the ratio estimates were formed from data segments corresponding to the largest available signal-to-noise ratios.

Appendix C: the directivity index

The directivity index (DI) compares the intensity of the maximum lobe of a beam pattern with the intensity of a uniform source radiating the same total power output. The total power Π radiated by a directional sound source through a cylindrical surface of small height Δz enclosing the source is obtained by integrating the free-space sound pressure $p_s(r,\theta)$, so that:

$$\Pi = \frac{1}{2\rho_o c}\int_0^{2\pi} p_s^2(r,\theta)\Delta z r\,\mathrm{d}\theta\,, \qquad \text{(C1)}$$

where ρ_o is the density of sound in air and c is the speed of sound in air. (Note: angles in Appendix C are in radians.)

We can split the function for the free-space sound pressure field into the directional factor, $H(\theta)$, and the on-axis pressure, $p_{s,axis}(r)$, as in equation 1, then rewrite the above relationship for power as:

$$\Pi = \frac{1}{2\rho_o c}\,p_{s,axis}^2(r)\Delta z r\int_0^{2\pi} H^2(\theta)\,\mathrm{d}\theta\,. \qquad \text{(C2)}$$

A uniform source that generates the same acoustic power, Π_u, can be represented relative to the pressure amplitude $P_u(r)$ at r meters from the uniform source by:

$$\Pi = \Pi_u = \frac{1}{2\rho_o c}\int_0^{2\pi} p_u^2(r)\Delta z r\,\mathrm{d}\theta = \frac{2\pi}{2\rho_o c}\,p_u^2(r)\Delta z r\,. \qquad \text{(C3)}$$

It follows that the directional source will have a greater intensity along its acoustic axis than will the uniform source. The ratio of these intensities therefore gives us a measure of the directional concentration of the acoustic power. This ratio, called the directivity, D, can be represented as:

$$D = \frac{p_{s,axis}^2(r)}{p_u^2(r)}\,. \qquad \text{(C4)}$$

Setting equation C2 equal to equation C3, we can now solve for this above ratio and rewrite this equation as:

$$D = \frac{2\pi}{\int_0^{2\pi} H^2(\theta)\,\mathrm{d}\theta}\,. \qquad \text{(C5)}$$

The directivity index, DI, is the decibel equivalent of this quantity:

$$\mathrm{DI} = 10\log D\,. \qquad \text{(C6)}$$

Solving this equation for some simple radiation patterns shows us both the utility and limitations of this index. For a pulsating sphere where $H(\theta)=0$, we find that DI=0 dB. A hemispherical source mounted on a rigid baffle where $H(\theta)=0$ for $0<\theta\leqslant\pi$ and $H(\theta)=0$ for $\pi<\theta\leqslant 2\pi$ then has DI=3.01 dB. For a simple dipole radiation pattern where $H(\theta)=\cos^2\theta$, we find an equivalent DI=3.01 dB. This illustrates that the directivity index does not inform us as to the shape of the radiation pattern, only the degree to which the acoustic power is concentrated.

To calculate the directivity index of the measured radiation patterns from our eight-point array, we solved for a measure of the squared directional factor, $H^2(\theta)$, and approximated the integration in equation C5 using Simpson's rule. Substituting into equation C6, we arrived at the final solution:

$$\mathrm{DI} = 10\log\frac{2\pi}{\frac{\pi}{12}\left\{4\sum_{j=1,3,5,7} H_j^2 + 2\sum_{k=0,2,4,6} H_k^2\right\}}\,, \qquad \text{(C7)}$$

where $H(2\pi)=H(0)$ and H_0 was defined as the point where $H(\theta)=1$. In practice, our measure of the squared directional factor was $H_{band}^2(\theta)$ from equation 8 or $H_{band,note}^2(\theta)$ from equation 10.

For simple beam patterns, this approximation should not overestimate the value of DI. The degree to which the calculation approximates the true value of DI is dependent on where the eight samples of the beam pattern are taken. To illustrate this, we used this equation to calculate the DI of the dipole radiation pattern, $H^2(\theta)=\cos^2\theta$, 10 000 times choosing the position of the first of eight equally spaced samples randomly from $0\leqslant\theta<\pi/4$. This yielded a range of values (median 2.84 dB; range 2.32 dB<DI<3.01 dB). No values exceed the value calculated analytically above. We therefore suggest that our approximation of the directivity index is a conservative measure of the directionality of the true beam pattern.

List of symbols

$b(\theta)$	the beam pattern, the decibel equivalent of the directional factor H (dB)
$b_{band}(\theta)$	band-averaged beam pattern (dB)
$b_{band,note}(\theta)$	time- and band-averaged beam pattern (dB)

c	speed of sound ($m\,s^{-1}$)
D	directivity, a measure of the directionality of the sound field (dimensionless)
DI	directivity index, the decibel equivalent of D (dB)
f	frequency of vibration (Hz)
$H(\theta)$	the directional factor, a normalized function (dimensionless)
$H_{band}^2(\theta)$	frequency-band average of the squared directional factor (dimensionless)
$H_{band,note}^2(\theta)$	time- and frequency-band average of the squared directional factor (dimensionless)
H_0	point where $H(\theta)=1$
mode[θ_{max}]	beam pattern modal maximum (degrees)
mode[θ_{min}]	beam pattern modal minimum (degrees)
n	number of time slices
p_r	spectral density of the acoustic pressure measured at the receivers ($Pa\,H^{-1/2}$)
p_s	spectral density of the acoustic pressure generated by a source ($Pa\,H^{-1/2}$)
$p_{s,axis}$	spectral density of the acoustic pressure on the acoustic axis ($Pa\,H^{-1/2}$)
p_u	spectral density of the acoustic field generated by a uniform source ($Pa\,H^{-1/2}$)
r	distance from source (m)
TL	transmission loss (dB)
V_g	signal generator voltage (V)
V_r	output voltage from the microphone amplifiers (V)
z	vertical distance (m)
α_s	source frequency response, a frequency-dependent constant ($Pa\,V^{-1}$)
α_r	receiver response, a frequency-independent constant ($Pa\,V^{-1}$)
Π	acoustic power (W)
Π_{band}	frequency-band average of the acoustic power (W)
Π_u	acoustic power generated by a uniform source (W)
θ	horizontal angle relative to the front of the source (degrees; radians in Appendix C)
θ_{max}	value of θ at which $b(\theta)$ is a maximum (degrees)
θ_{min}	value of θ at which $b(\theta)$ is a minimum (degrees)
ρ_o	density ($kg\,m^{-3}$)

This work was supported by the National Science Foundation through a Graduate Research Fellowship (M.S.D.), a Doctoral Dissertation Research Grant IBN-9701201 (M.S.D. and J.W.B.) and grant IBN-9406217 (J.W.B.). We received additional field study support from a Mildred E. Mathias Graduate Student Research Grant through the University of California's Natural Reserve System (M.S.D.). Additional support was provided by NIH training grant T32GM-07240 (M.S.D.) and the US Office of Naval Research (G.B.D.). We thank the Sierra Nevada Aquatic Research Laboratory and Dan Dawson for providing field facilities and the Bureau of Land Management (Bishop, CA, USA) and Terry Russi for access to the field site. We thank Dahlia Chazan for her excellent assistance in the field. We thank Catherine DeRivera, Darren Irwin, Dr Jules Jaffe and two anonymous reviewers for critical comments on the manuscript and also Kathryn Cortopassi, Jami Dantzker and Alejandro Purgue for helpful discussions.

References

Archibald, H. L. (1974). Directional differences in the sound intensity of ruffed grouse drumming. *Auk* **91**, 517–521.

Au, W. W., Pawloski, J. L., Nachtigall, P. E., Blonz, M. and Gisner, R. C. (1995). Echolocation signals and transmission beam pattern of a false killer whale (*Pseudorca crassidens*). *J. Acoust. Soc. Am.* **98**, 51–9.

Bennet-Clark, H. C. (1987). The tuned singing burrow of mole crickets. *J. Exp. Biol.* **128**, 383–409.

Bradbury, J. W. and Vehrencamp, S. L. (1998). *Principles of Animal Communication*. Sunderland, MA: Sinauer Associates.

Brenowitz, E. A. (1982). The active space of red-winged blackbird song. *J. Comp. Physiol.* A **147**, 511–522.

Embleton, T. F. W. (1996). Tutorial on sound propagation outdoors. *J. Acoust. Soc. Am.* **100**, 31–48.

Embleton, T. F. W., Piercy, J. E. and Daigle, G. A. (1983). Effective flow resistivity of ground surfaces determined by acoustical measurements. *J. Acoust. Soc. Am.* **74**, 1239–1244.

Embleton, T. F. W., Piercy, J. E. and Olson, N. (1976). Outdoor sound propagation over ground of finite impedance. *J. Acoust. Soc. Am.* **59**, 267–277.

Flanagan, J. L. (1972). *Speech Analysis; Synthesis and Perception*. New York: Springer-Verlag.

Forrest, T. G. (1991). Power output and efficiency of sound production by crickets. *Behav. Ecol.* **2**, 327–338.

Forrest, T. G. (1994). From sender to receiver: Propagation and environmental effects on acoustic signals. *Am. Zool.* **34**, 644–654.

Forrest, T. G. and Raspet, R. (1994). Models of female choice in acoustic communication. *Behav. Ecol.* **5**, 293–303.

Freitag, L. E. and Tyack, P. L. (1993). Passive acoustic localization of the Atlantic bottlenose dolphin using whistles and echolocation clicks. *J. Acoust. Soc. Am.* **93**, 2197–2205.

Fuzessery, Z. M., Hartley, D. J. and Wenstrup, J. J. (1992). Spatial processing within the mustache bat echolocation system – possible mechanisms for optimization. *J. Comp. Physiol.* A **170**, 57–71.

Gerhardt, H. C. (1975). Sound pressure levels and radiation patterns of the vocalizations of some North American frogs and toads. *J. Comp. Physiol.* **102**, 1–12.

Gerhardt, H. C. (1998). Acoustic signals of animals: recording, field measurements, analysis and description. In *Animal Acoustic Communication: Sound Analysis and Research Methods* (ed. S. L. Hopp, M. J. Owren and C. S. Evans), pp. 1–25. Berlin, New York: Springer.

Gibson, R. M. (1996). Female choice in sage grouse: the roles of attraction and active comparison. *Behav. Ecol. Sociobiol.* **39**, 55–59.

Gibson, R. M. and Bradbury, J. W. (1985). Sexual selection in lekking grouse: phenotypic correlates of male strutting success. *Behav. Ecol. Sociobiol.* **18**, 117–123.

Gibson, R. M., Bradbury, J. W. and Vehrencamp, S. L. (1991). Mate choice in lekking sage grouse revisited: the roles of

vocal display, female site fidelity and copying. *Behav. Ecol.* **2**, 165–180.

Hartley, D. J. and Suthers, R. A. (1987). The sound emission pattern and the acoustical role of the noseleaf in the echolocating bat, *Carolia perspicillata*. *J. Acoust. Soc. Am.* **82**, 1892–1900.

Hartley, D. J. and Suthers, R. A. (1989). The sound emission pattern of the echolocating bat, *Eptesicus fuscus*. *J. Acoust. Soc. Am.* **85**, 1348–1351.

Hartley, D. J. and Suthers, R. A. (1990). Sonar pulse radiation and filtering in the mustached bat, *Pteronotus parnellii rubiginosus*. *J. Acoust. Soc. Am.* **87**, 2756–2772.

Hartzler, J. E. (1972). An analysis of sage grouse lek behavior. PhD thesis, University of Montana, Missoula, USA.

Hjorth, I. (1970). Reproductive behavior in Tetranidae, with special reference to males. *Viltrevy* **7**, 183–596.

Höglund, J. and Alatalo, R. V. (1995). Leks. In *Monographs in Behavior and Ecology* (ed. J. R. Krebs and T. Clutton-Brock), xiii, 248p. Princeton, NJ: Princeton University Press.

Honess, R. F. and Allred, W. J. (1942). Structure and function of the neck muscles in inflation and deflation of the esophagus in the sage cock. *Wyoming Game Fish Dept Bull.*, no. 2, 5–12.

Hunter, M. L. J., Kacelnik, A., Roberts, J. and Vuillermoz, M. (1986). Directionality of avian vocalizations: a laboratory study. *Condor* **88**, 371–375.

Kinsler, L. E., Frey, A. R., Coppens, A. B. and Sanders, J. V. (1982). *Fundamentals of Acoustics*. New York: Wiley.

Klump, G. M. and Shalter, M. D. (1984). Acoustic behaviour of birds and mammals in the predator context. I. Factors affecting the structure of alarm signals. II. The functional significance and evolution of alarm signals. *Z. Tierpsychol.* **66**, 189–226.

Larsen, O. N. and Dabelsteen, T. (1990). Directionality of blackbird vocalization. Implications for vocal communication and its further study. *Ornis Scand.* **21**, 37–45.

Lumsden, H. G. (1968). The displays of the sage grouse. *Ontario Department of Lands and Forests Reseach Report (Wildlife)* **83**, 1–94.

MathWorks (1998). *MATLAB*. Natick, MA: Math Works Inc.

McGregor, P. K., Dabelsteen, T., Clark, C. W., Bower, J. L., Tavares, J. P. and Holland, J. (1997). Accuracy of a passive acoustic location system: empirical studies in terrestrial habitats. *Ethol. Ecol. Evol.* **9**, 269–286.

McGregor, P. K. and Krebs, J. R. (1984). Sound degradation as a distance cue in great tit (*Parus major*) song. *Behav. Ecol. Sociobiol.* **16**, 49–56.

Mogensen, F. and Møhl, B. (1979). Sound radiation patterns in the freqency domain of cries from a vespertilionid bat. *J. Comp. Physiol.* A **134**, 165–171.

Möhres, F. P. (1967). Ultrasonic orientation in megadermatic bats. In *Animal Sonar Systems: Biology and Bionics*, vol. 1 (ed. R. G. Busnel), pp. 115–127. France: Laboratoire de Physiologie Acoustique.

Narins, P. M. and Hurley, D. D. (1982). The relationship between call intensity and function in the Puerto Rican coqui (Anura: Leptodactylidae). *Herpetologica* **38**, 287–295.

Passmore, N. I. (1981). Sound levels of mating calls of some African frogs. *Herpetologica* **37**, 166–171.

Patterson, R. L. (1952). *The Sage Grouse in Wyoming*. Denver, CO: Sage Books.

Piercy, J. E. and Embelton, T. F. W. (1977). Review of noise propagation in the atmosphere. *J. Acoust. Soc. Am.* **61**, 1403–1418.

Pilleri, G. (1990). Adaptation to water and the evolution of echolocation in the Cetacea. *Ethol. Ecol. Evol.* **2**, 135–163.

Pilleri, G., Zbinden, K., Gihr, M. and Kraus, C. (1976). Sonar clicks, directionality of the emission field and echolocating behaviour of the Indus River Dolphin (*Platanista indi* Blyth, 1859). In *Investigations on Cetacea*, vol. X (ed. G. Pilleri), pp. 157–188. Berne: Brain Anatomy Institute.

Prestwich, K. N. (1994). The energetics of acoustic signaling in anurans and insects. *Am. Zool.* **34**, 625–643.

Prestwich, K. N., Brugger, K. E. and Topping, M. (1989). Energy and communication in three species of hylid frogs: power input, power output and efficiency. *J. Exp. Biol.* **144**, 53–80.

Purves, P. E. and Pilleri, G. E. (1983). *Echolocation in Whales and Dolphins*. New York: Academic Press.

Richards, D. G. (1981). Estimation of distance of singing conspecifics by the Carolina wren. *Auk* **98**, 127–133.

Schnitzler, H.-U. and Henson, O. W. (1980). Performance of airborne animals sonar systems. I. Microchiroptera. In *Animal Sonar Systems* (ed. R. G. Busnel and J. D. Fish), pp. 801–827. New York: Plenum.

Scott, J. W. (1942). Mating behavior of the sage grouse. *Auk* **59**, 477–498.

Shure, L. and McClellan, J. (1997). *XCORR Cross-Correlation Function Estimates*. Natick, MA: Math Works Inc.

Simon, J. R. (1940). Mating performance of the sage grouse. *Auk* **57**, 467–471.

Sokolov, B. V. and Makarov, A. K. (1971). Direction of the ultrasonic radiation and role of the nasal leaf in *Rhinolophus ferrumequinum*. *Biologicheskie Nauki* **7**, 37–44.

Spiesberger, J. L. and Fristrup, K. M. (1990). Passive localization of calling animals and sensing of their acoustic environment using acoustic tomography. *Am. Nat.* **135**, 107–153.

Spurrier, M. F., Boyce, M. S. and Manly, B. F. J. (1994). Lek behaviour in captive sage grouse *Centrocercus urophasianus*. *Anim. Behav.* **47**, 303–310.

Stevens, K. N. (1997). Models of speech production. In *Encyclopedia of Acoustics*, vol. 4 (ed. M. J. Crocker), pp. 1565–1578. New York: Wiley.

Strother, G. K. and Mogus, M. (1970). Acoustical beam patterns for bats: Some theoretical considerations. *J. Acoust. Soc. Am.* **48**, 1430–1432.

Watkins, A. W. and Schevill, W. E. (1971). Four hydrophone array for acoustic three-dimensional location. *Woods Hole Oceanographic Institute Technical Report* 71-60.

Watkins, W. A. and Schevill, W. E. (1972). Sound source location by arrival-times on a non-rigid three-dimensional hydrophone array. *Deep-Sea Res.* **19**, 691–706.

Wiley, R. H. (1973a). The strut diplay of male sage grouse: a 'fixed' action pattern. *Behaviour* **47**, 129–152.

Wiley, R. H. (1973b). Territoriality and non-random mating in sage grouse, *Centrocercus urophasianus*. *Anim. Behav. Monogr.* **6**, 85–169.

Witkin, S. R. (1977). The importance of directional sound radiation in avian vocalization. *Condor* **79**, 490–493.

Wotton, J. M., Jenison, R. L. and Hartley, D. J. (1997). The combination of echolocation emission and ear reception enhances directional spectral cues of the big brown bat, *Eptesicus fuscus*. *J. Acoust. Soc. Am.* **101**, 1723–1733.

Young, J. R. (1994). The influence of sexual selection on phenotypic and genetic divergence among sage grouse populations. PhD thesis, Purdue University, USA.

Young, J. R., Hupp, J. W., Bradbury, J. W. and Braun, C. E. (1994). Phenotypic divergence of secondary sexual traits among sage grouse, *Centrocercus urophasianus*, populations. *Anim. Behav.* **47**, 1353–1362.